

# The Effective Standard Model after LHC Run I

John Ellis<sup>1,2</sup>, Verónica Sanz<sup>3</sup> and Tevong You<sup>1</sup>

<sup>1</sup>*Theoretical Particle Physics and Cosmology Group, Physics Department,  
King's College London, London WC2R 2LS, UK*

<sup>2</sup>*TH Division, Physics Department, CERN, CH-1211 Geneva 23, Switzerland*

<sup>3</sup>*Department of Physics and Astronomy, University of Sussex, Brighton BN1 9QH, UK*

## Abstract

We treat the Standard Model as the low-energy limit of an effective field theory that incorporates higher-dimensional operators to capture the effects of decoupled new physics. We consider the constraints imposed on the coefficients of dimension-6 operators by electroweak precision tests (EWPTs), applying a framework for the effects of dimension-6 operators on electroweak precision tests that is more general than the standard  $S, T$  formalism, and use measurements of Higgs couplings and the kinematics of associated Higgs production at the Tevatron and LHC, as well as triple-gauge couplings at the LHC. We highlight the complementarity between EWPTs, Tevatron and LHC measurements in obtaining model-independent limits on the effective Standard Model after LHC Run 1. We illustrate the combined constraints with the example of the two-Higgs doublet model.

October 2014

# 1 Introduction

Run 1 of the LHC has taken probes of the Standard Model to a new level, not only by the discovery of the Higgs boson  $H(125)$  [1] and the absence of other new particles, but also via the new constraints imposed on the couplings of vector bosons and the top quark [2]. Now is an appropriate time to assess the global constraints placed on possible new physics by LHC Run 1 in conjunction with the Tevatron, LEP and other experiments. In view of the kinematic reach of the LHC, it is natural to suppose that the threshold for any new physics may lie substantially above the masses of the Standard Model particles. In this case, the new physics may be analyzed in the decoupling limit [3], and its effects may be parameterized in terms of higher-dimensional operators composed of Standard Model fields [4]. Using the equations of motions reduces the number of independent operators [5], with a complete non-redundant set first categorised in [6].

This is the effective Standard Model approach adopted in a large number of recent papers<sup>1</sup> [8, 9], and there have been many analyses of the constraints imposed on new physics via upper limits on the coefficients of a complete dimension-6 operator basis [10–14], in particular. Several different classes of measurements make important contributions to these constraints. LEP and other experiments contribute via electroweak precision tests (EWPTs) [15], which are often presented as constraints on the  $S$  and  $T$  parameters that are defined in terms of oblique radiative corrections due to vacuum polarization diagrams, and via measurements of triple-gauge couplings (TGCs). The Tevatron experiments contribute via measurements of (constraints on) production of the Higgs boson  $H$  in association with massive gauge bosons  $V = W^\pm, Z^0$  [16]. Finally, the LHC experiments contribute via many Higgs measurements including signal strengths [17], branching ratios and kinematic distributions [18], and also via TGC measurements [19, 20].

We demonstrated in previous work [14] the power of the constraints provided by measurements of kinematic distributions in  $V + H$  production at the Tevatron and the LHC, showing that measurements of the  $V + H$  invariant mass  $M_{VH}$  at the Tevatron and the transverse momentum  $p_T^V$  at the LHC could close off a ‘blind’ direction in the parameter space of dimension-6 operator coefficients that had been allowed by previous analyses of LEP and LHC data [21]. Subsequently, new data on TGCs from LHC running at 8 TeV have been published [19, 20]. In this paper we make the first complete analysis of the data from LHC Run 1 and the Tevatron, in combination with the EWPT constraints, considering only CP-even operators and assuming minimal flavour violation. The dimension-6 operators we consider and the 95% CL ranges that we find for their coefficients are listed in Tables 1 and 2.

We confirm previous findings that the EWPTs place very strong constraints on certain (combinations of) operator coefficients. On the other hand, we also find that the Higgs observables (signal strengths and associated production kinematics) and the TGC measurements at the LHC also have complementary rôles to play. Some operator coefficients are better constrained by the TGC data, and some by the Higgs data. One coefficient in particular only affects TGCs and nothing else. Only their combination provides a complete picture of the constraints on the dimension-6 operator coefficients after LHC Run 1.

The outline of this paper is as follows. In Section 2 we discuss the EWPTs, first reviewing a general expansion formalism for EWPTs, and then demonstrating that it reproduces the constraints on the vacuum polarization parameters  $S$  and  $T$  found in other analyses before illustrating its use in capturing the effects of a complete basis of dimension-6 operators. In Section 3 we discuss the constraints imposed by measurements of Higgs couplings, associated

---

<sup>1</sup>For earlier studies of dimension-6 operators in triple-gauge couplings and Higgs physics see for example [7].

Higgs production kinematics and TGCs at the LHC, demonstrating their complementarity. Section 4 illustrates the application of these combined constraints on the coefficients of dimension-6 operators to the two-Higgs-doublet model (2HDM). Section 5 summarizes our conclusions and assesses some future prospects, and an Appendix discusses aspects of kinematics and the applicability of effective field theory in our analysis.

## 2 Electroweak Precision Tests at LEP

Electroweak precision tests (EWPTs), particularly those provided by LEP, are amongst the most sensitive observables for constraining new physics beyond the Standard Model. EWPTs are typically summarized via constraints on the  $S$  and  $T$  parameters [22] and their generalization to include the  $W$  and  $Y$  parameters [23] that are relevant for custodially-symmetric and weak isospin-preserving new physics, which characterize the Standard Model vector boson self-energy corrections<sup>2</sup>. If new physics affects only the Standard Model gauge sector and does not couple directly to Standard Model fermions, this approach may be sufficient for placing bounds on such ‘universal’ models, but the effective Standard Model also includes fermionic operators that affect electroweak precision tests. Thus a more general framework is required to capture all the possible effects of decoupled new physics in a model-independent way.

There have been many studies considering individual or subsets of bounds for all dimension-6 operators entering in EWPTs, for example [25, 26], and full analyses including simultaneously a complete basis of dimension-6 operators affecting these EWPTs have been performed in [10, 12, 13], but a full calculation of the effects of propagation of corrections to input observables and self-energies as well as direct contributions to observables was needed in each different basis. Here we employ instead the recent expansion formalism of [27], which separates the calculation of the corrections’ effects on the EWPT observables and the calculations of the contributions to the corrections from new physics. This framework facilitates any  $\chi^2$  analysis that seeks to go beyond the  $S, T$  parametrization and renders more transparent the origin of the effects from each operator.

### 2.1 The Expansion Formalism

For convenience, we briefly summarize here the analysis of [27]. The principle is that, given the Standard Model with Lagrangian parameters  $p_{\text{SM}} \equiv \{g, g', g_s, y_t, v, \lambda\}$ , one may calculate theoretical values  $\hat{\mathcal{O}}_i^{\text{th}}(p_{\text{SM}})$  for the observables

$$\hat{\mathcal{O}}_i \equiv \{m_Z, G_F, \alpha(m_Z), m_t, \alpha_s, m_H, m_W, \Gamma_l, \Gamma_q, \sigma_{\text{had}}, R_l, \sin^2 \theta_{\text{eff}}, A_f, A_{FB}^f, \dots\}$$

that are measured by experiments with errors  $\Delta \hat{\mathcal{O}}_i^{\text{exp}}$ . To compare the theoretical predictions  $\hat{\mathcal{O}}_i^{\text{th}}(p_{\text{SM}})$  with the experimental measurements,  $\hat{\mathcal{O}}_i^{\text{exp}}$ , we must first choose 6 of these observables as ‘input’ observables  $\hat{\mathcal{O}}_{i'}$ , typically the most precisely measured ones<sup>3</sup>, such as

$$\hat{\mathcal{O}}_{i'} \equiv \{m_Z, G_F, \alpha(m_Z), m_t, \alpha_s, m_H\}.$$

These assign values  $p_{\text{SM}}^{\text{ref}}$  to the Lagrangian parameters such that the  $\hat{\mathcal{O}}_{i'}^{\text{th}}(p_{\text{SM}}^{\text{ref}})$  agree well with measurements, and numerical values for the other ‘output’ observables can then be obtained in terms of  $p_{\text{SM}}^{\text{ref}}$ .

<sup>2</sup>See also [24] for another parametrisation of EWPT fits that includes vertex corrections in a set of  $\epsilon$  parameters.

<sup>3</sup>Another convenient choice of input observables is to use  $m_W$  instead of  $G_F$  [28].

In the presence of new physics characterized by parameters  $p_\alpha$ , the theoretical expressions for the observables are modified by a correction  $\delta^{\text{NP}}\hat{\mathcal{O}}_i(p_{\text{SM}}, p_\alpha)$ :

$$\hat{\mathcal{O}}_i^{\text{th}}(p_{\text{SM}}, p_\alpha) = \hat{\mathcal{O}}_i^{\text{SM}}(p_{\text{SM}}) + \delta^{\text{NP}}\hat{\mathcal{O}}_i(p_{\text{SM}}, p_\alpha).$$

Since the relations between input observables and Lagrangian parameters are modified in general, a different  $p_{\text{SM}}^{\text{ref}}$  value would normally be preferred to compensate for non-zero values of  $p_\alpha$  so as to remain in agreement with experiment. This may be quantified by a  $\chi^2$  analysis that varies the parameters  $(p_{\text{SM}}, p_\alpha)$  so as to minimize the function

$$\chi^2(p_{\text{SM}}, p_\alpha) = \sum_{i,j} (\hat{\mathcal{O}}_i^{\text{th}} - \hat{\mathcal{O}}_i^{\text{exp}})(\sigma^2)_{ij}^{-1} (\hat{\mathcal{O}}_j^{\text{th}} - \hat{\mathcal{O}}_j^{\text{exp}}) \quad , \quad (\sigma^2)_{ij} = \Delta\hat{\mathcal{O}}_i^{\text{exp}} \rho_{ij} \Delta\hat{\mathcal{O}}_j^{\text{exp}} \quad ,$$

where  $\rho_{ij}$  is the correlation matrix.

To avoid recomputing the full expression  $\hat{\mathcal{O}}_i^{\text{th}}(p_{\text{SM}}, p_\alpha)$  for each value of  $p_{\text{SM}}$  and  $p_\alpha$ , the expansion formalism involves expanding about the Standard Model reference values for the Lagrangian parameters:

$$\begin{aligned} \hat{\mathcal{O}}_i^{\text{SM}}(p_{\text{SM}}) &= \hat{\mathcal{O}}_i^{\text{SM}}(p_{\text{SM}}^{\text{ref}}) + \sum_{p_{\text{SM}}} \frac{\partial \hat{\mathcal{O}}_i^{\text{SM}}}{\partial p_{\text{SM}}} (p_{\text{SM}} - p_{\text{SM}}^{\text{ref}}) + \dots \\ &\simeq \hat{\mathcal{O}}_i^{\text{ref}} [1 + \bar{\delta}^{\text{SM}} \hat{\mathcal{O}}_i(p_{\text{SM}})] \quad , \end{aligned}$$

where  $\hat{\mathcal{O}}_i^{\text{ref}} \equiv \hat{\mathcal{O}}_i^{\text{SM}}(p_{\text{SM}}^{\text{ref}})$ ,  $\bar{\delta}^{\text{SM}} \hat{\mathcal{O}}_i(p_{\text{SM}}) = \sum_{p_{\text{SM}}} G_{ip_{\text{SM}}} \bar{\delta} p_{\text{SM}}$ , and the quantities  $G_{ik'} \equiv \frac{p_{\text{SM}}^{\text{ref}}}{\hat{\mathcal{O}}_i^{\text{ref}}} \frac{\partial \hat{\mathcal{O}}_i^{\text{SM}}}{\partial p_{\text{SM}}}$  are expansion coefficients that need only to be calculated once. Here  $\bar{\delta} p_{\text{SM}} \equiv (p_{\text{SM}} - p_{\text{SM}}^{\text{ref}})/p_{\text{SM}}^{\text{ref}}$ , and the fractional shift  $\bar{\delta}$  is defined in general as  $\bar{\delta} \hat{\mathcal{O}}_i \equiv (\hat{\mathcal{O}}_i - \hat{\mathcal{O}}_i^{\text{ref}})/\hat{\mathcal{O}}_i^{\text{ref}}$ . Furthermore, to emphasize that the  $p_{\text{SM}}$  are not directly measurable, but are determined from the input observables  $\hat{\mathcal{O}}_{i'}$ , we note that the Lagrangian parameters can be eliminated in favour of the input observables by inverting the relation  $\bar{\delta}^{\text{SM}} \hat{\mathcal{O}}_{i'} = \sum_{p_{\text{SM}}} G_{i'p_{\text{SM}}} \bar{\delta} p_{\text{SM}}$ , so that

$$\bar{\delta}^{\text{SM}} \hat{\mathcal{O}}_i = \sum_{i'} G_{ip_{\text{SM}}} \left( \sum_{p_{\text{SM}}} (G^{-1})_{p_{\text{SM}}i'} \bar{\delta}^{\text{SM}} \hat{\mathcal{O}}_{i'} \right) = \sum_{i'} d_{ii'} \bar{\delta}^{\text{SM}} \hat{\mathcal{O}}_{i'} \quad . \quad (2.1)$$

The expansion coefficients for the output observables in terms of input observables are then given by the matrix  $d_{ii'} \equiv \sum_{p_{\text{SM}}} G_{ip_{\text{SM}}} (G^{-1})_{p_{\text{SM}}i'}$ .

The theoretical predictions for the output observables can now be written as  $\hat{\mathcal{O}}_i^{\text{th}} = \hat{\mathcal{O}}_i^{\text{ref}}(1 + \bar{\delta} \hat{\mathcal{O}}_i^{\text{th}})$ , with

$$\bar{\delta} \hat{\mathcal{O}}_i^{\text{th}} = \sum_{i'} d_{ii'} \bar{\delta}^{\text{SM}} \hat{\mathcal{O}}_{i'} + \xi_i = \sum_{i'} d_{ii'} (\bar{\delta} \hat{\mathcal{O}}_{i'}^{\text{th}} - \xi_{i'}) + \xi_i \quad ,$$

where we used  $\bar{\delta} \hat{\mathcal{O}}_{i'}^{\text{SM}} = \bar{\delta} \hat{\mathcal{O}}_{i'}^{\text{th}} - \xi_{i'}$  and defined  $\xi_i \equiv \delta^{\text{NP}} \hat{\mathcal{O}}_i / \hat{\mathcal{O}}_i^{\text{ref}}$ . The  $d_{ii'}$  matrix is pre-calculated and encapsulates the dependence of each output observable on each input observable, so that one needs only to plug in the contribution due to new physics that affect the input observables,  $\xi_{i'}$ , and those that directly affect the output observables,  $\xi_i$ . We note that, for the case of vector boson self-energy corrections, the  $\pi_{VV} \equiv \{\pi_{ZZ}, \pi'_{ZZ}, \pi_{\gamma Z}, \pi'_{\gamma\gamma}, \pi_{+-}, \pi_{WW}^0\}$  are defined as in [27], and the contributions to output observables through  $\xi_{i'}$  and  $\xi_i$  are summarized by the given  $b_{i,VV}$  coefficients. We then have

$$\bar{\delta} \hat{\mathcal{O}}_i^{\text{th}} = \sum_{i'} d_{ii'} \bar{\delta} \hat{\mathcal{O}}_{i'}^{\text{th}} + \bar{\delta}^{\text{NP}} \hat{\mathcal{O}}_i \quad ,$$

where

$$\delta^{\text{NP}} \hat{\mathcal{O}}_i \equiv \xi_i - \sum_{i'} d_{ii'} \xi_{i'} + \sum_{VV} b_{i,VV} \delta^{\text{NP}} \pi_{VV}, \quad (2.2)$$

and it remains only to determine the  $\xi_{i'}$ ,  $\xi_i$  and  $\delta^{\text{NP}} \pi_{VV}$  from the dimension-6 operators in the effective Standard Model.

## 2.2 Dimension-6 Operators in EWPTs

Operator	Coefficient	LEP Constraints	
		Individual	Marginalized
$\mathcal{O}_W = \frac{ig}{2} \left( H^\dagger \sigma^a \overleftrightarrow{D}^\mu H \right) D^\nu W_{\mu\nu}^a$ $\mathcal{O}_B = \frac{ig'}{2} \left( H^\dagger \overleftrightarrow{D}^\mu H \right) \partial^\nu B_{\mu\nu}$	$\frac{m_W^2}{\Lambda^2} (c_W + c_B)$	(-0.00055, 0.0005)	(-0.0033, 0.0018)
$\mathcal{O}_T = \frac{1}{2} \left( H^\dagger \overleftrightarrow{D}_\mu H \right)^2$	$\frac{v^2}{\Lambda^2} c_T$	(0, 0.001)	(-0.0043, 0.0033)
$\mathcal{O}_{LL}^{(3)l} = (\bar{L}_L \sigma^a \gamma^\mu L_L) (\bar{L}_L \sigma^a \gamma_\mu L_L)$	$\frac{v^2}{\Lambda^2} c_{LL}^{(3)l}$	(0, 0.001)	(-0.0013, 0.00075)
$\mathcal{O}_R^e = (i H^\dagger \overleftrightarrow{D}_\mu H) (\bar{e}_R \gamma^\mu e_R)$	$\frac{v^2}{\Lambda^2} c_R^e$	(-0.0015, 0.0005)	(-0.0018, 0.00025)
$\mathcal{O}_R^u = (i H^\dagger \overleftrightarrow{D}_\mu H) (\bar{u}_R \gamma^\mu u_R)$	$\frac{v^2}{\Lambda^2} c_R^u$	(-0.0035, 0.005)	(-0.011, 0.011)
$\mathcal{O}_R^d = (i H^\dagger \overleftrightarrow{D}_\mu H) (\bar{d}_R \gamma^\mu d_R)$	$\frac{v^2}{\Lambda^2} c_R^d$	(-0.0075, 0.0035)	(-0.042, 0.0044)
$\mathcal{O}_L^{(3)q} = (i H^\dagger \sigma^a \overleftrightarrow{D}_\mu H) (\bar{Q}_L \sigma^a \gamma^\mu Q_L)$	$\frac{v^2}{\Lambda^2} c_L^{(3)q}$	(-0.0005, 0.001)	(-0.0044, 0.0044)
$\mathcal{O}_L^q = (i H^\dagger \overleftrightarrow{D}_\mu H) (\bar{Q}_L \gamma^\mu Q_L)$	$\frac{v^2}{\Lambda^2} c_L^q$	(-0.0015, 0.003)	(-0.0019, 0.0069)

**Table 1:** List of operators and coefficients in our basis entering in EWPTs at LEP, together with 95% CL bounds when individual coefficients are switched on one at a time, and marginalized in a simultaneous fit. For the first four coefficients we report the constraints from the leptonic observables, while the remaining coefficients also include the hadronic observables.

We begin with the familiar  $S, T$  parameters before generalizing to a complete dimension-6 operator basis. The universal parts of new physics contributions are often parametrized as oblique corrections to vector boson self-energies, which can be written in terms of gauge eigenstates as

$$\mathcal{L}_{\text{VV}} = -W^{+\mu} \pi_{+-}(p^2) W_\mu^- - \frac{1}{2} W^{3\mu} \pi_{33}(p^2) W_\mu^3 - W^{3\mu} \pi_{3B}(p^2) B_\mu - \frac{1}{2} B^\mu \pi_{BB}(p^2) B_\mu,$$

where  $\pi_{VV}(p^2) = \pi_{VV}^{\text{SM}}(p^2) + \delta\pi_{VV}(p^2)$ . Making a Taylor expansion at the quadratic order to which dimension-6 operators can contribute:

$$\pi_{VV}(p^2) = \pi_{VV}(0) + p^2 \pi'_{VV}(0) + \frac{1}{2} (p^2)^2 \pi''_{VV}(0) + \dots,$$

the usual  $\hat{S}$  and  $\hat{T}$  parameters <sup>4</sup> can be defined as

$$\hat{S} \equiv \frac{g}{g'} \frac{\pi'_{3B}(0)}{\pi'_{+-}(0)} \quad , \quad \hat{T} \equiv \frac{\pi_{+-}(0) - \pi_{33}(0)}{\pi_{+-}(0)} .$$

Since  $U(1)_Q$  symmetry is conserved, which requires  $\pi_{\gamma\gamma}(0)$  and  $\pi_{\gamma Z}(0)$  to vanish by gauge invariance, the following relations must hold:

$$\begin{aligned} g'^2 \pi_{33}(0) + g^2 \pi_{BB}(0) + 2gg' \pi_{3B}(0) &= 0 \\ g \pi_{BB}(0) + g' \pi_{3B}(0) &= 0 . \end{aligned}$$

After normalizing the  $W^\pm$  and  $B$  fields so that the kinetic terms are canonical and  $\pi_{+-}(0) = -m_W^2$ , we obtain the following  $\hat{S}$  and  $\hat{T}$  corrections in the gauge mass eigenstates for the quantities  $\delta^{\text{NP}} \pi_{VZ}$  defined in [27]:

$$\begin{aligned} \delta^{\text{NP}} \pi_{ZZ} &= -\hat{T} + 2\hat{S} \sin^2 \theta_W \\ \delta^{\text{NP}} \pi'_{ZZ} &= 2\hat{S} \sin^2 \theta_W \\ \delta^{\text{NP}} \pi_{\gamma Z} &= -\hat{S} \cos 2\theta_W \tan \theta_W \\ \delta^{\text{NP}} \pi'_{\gamma\gamma} &= -2\hat{S} \sin^2 \theta_W . \end{aligned}$$

Inserting these expressions into (2.2) and performing a  $\chi^2$  analysis in the expansion formalism, using as output observables the EWPTs at the  $Z$  peak and the  $W$  mass:

$$\hat{\mathcal{O}}_i = \{ \Gamma_Z, \sigma_{\text{had}}^0, R_e^0, R_\mu^0, R_\tau^0, A_{\text{FB}}^{0,e}, \sin^2 \theta_{\text{eff}}^e, R_b^0, R_c^0, A_{\text{FB}}^{0,b}, A_{\text{FB}}^{0,c}, A_b, A_c, \sin^2 \theta_{\text{eff}}^b, \sin^2 \theta_{\text{eff}}^c, m_W \} ,$$

we obtain the 68%, 95%, and 99% CL allowed regions for  $S$  vs  $T$  shown in Fig. 1, denoted by dotted, dashed and solid contours respectively. We treat the observables as uncorrelated but have checked that including the correlation matrix, for example in the leptonic subset as given in [15], does not affect substantially our results, which agree reasonably closely with those of [29].

The  $\hat{S}$  and  $\hat{T}$  parameters are equivalent to a subset of the full set of dimension-6 operators that can affect the EWPTs. In a redundant basis those entering in oblique corrections to vector boson self-energies are

$$\mathcal{L}_{\text{dim-6}} \supset \frac{\bar{c}_{WB}}{m_W^2} \mathcal{O}_{WB} + \frac{\bar{c}_W}{m_W^2} \mathcal{O}_W + \frac{\bar{c}_B}{m_W^2} \mathcal{O}_B + \frac{\bar{c}_T}{v^2} \mathcal{O}_T + \frac{\bar{c}_{2W}}{m_W^2} \mathcal{O}_{2W} + \frac{\bar{c}_{2B}}{m_W^2} \mathcal{O}_{2B} ,$$

while those that affect the leptonic and hadronic  $Z$ -pole measurements directly through modifications to the gauge boson-fermion couplings are

$$\mathcal{L}_{\text{dim-6}} \supset \sum_{f_L} \left( \frac{\bar{c}_{f_L}}{v^2} \mathcal{O}_{f_L} + \frac{\bar{c}_{f_L}^{(3)}}{v^2} \mathcal{O}_{f_L}^{(3)} \right) + \sum_{f_R} \frac{\bar{c}_{f_R}}{v^2} \mathcal{O}_{f_R} .$$

The sum is over the left-handed lepton and quark doublets,  $f_L \equiv L_L, Q_L$ , and right-handed lepton and quark singlets,  $f_R \equiv e_R, u_R, d_R$ , and we assume minimal flavour violation. The

---

<sup>4</sup>These are related to the  $S$  and  $T$  parameters defined in [22] via  $S = \frac{4 \sin^2 \theta_W}{\alpha(m_Z)} \hat{S} \approx 119 \hat{S}$  and  $T = \frac{1}{\alpha(m_Z)} \hat{T} \approx 129 \hat{T}$ .

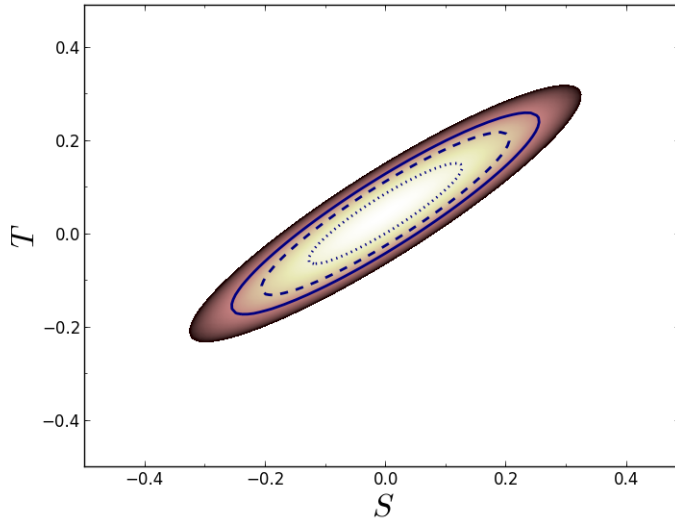


**Figure 1:** Results of a  $\chi^2$  analysis of  $ST$  parameters in EWPTs using the expansion formalism of [27]. The dotted, dashed and solid contours denote the regions allowed at the 68%, 95%, and 99% CL, respectively, which may be compared with those of [29].

Fermi constant  $G_F$  defined by the muon lifetime, which we take as an input observable, is modified by  $\bar{c}_{LL}^{(3)l}$  via the four-fermion operators  $\mathcal{O}_{LL}^{(3)l}$ :

$$\mathcal{L}_{\text{dim-6}} \supset \frac{\bar{c}_{LL}^{(3)l}}{v^2} \mathcal{O}_{LL}^{(3)l} .$$

We note that the coefficients are defined such that

$$\bar{c} \equiv c \frac{M^2}{\Lambda^2} , \quad (2.3)$$

where  $M \equiv v, m_W$  depending on the operator normalization, and  $c \sim g_{\text{NP}}^2$  is a coefficient proportional to a new physics coupling  $g_{\text{NP}}$  defined at the scale  $M$ . These are related to the coefficients at the new physics scale through RGE equations [31].

These operators form a redundant basis that is reducible through field redefinitions, or equivalently the equations of motion, that have no effect on the S-matrix [5]. Following [13], we may eliminate the operators  $\mathcal{O}_{LL}, \mathcal{O}_{LL}^{(3)}$  that affect the left-handed leptonic  $Z$  couplings, and the operators  $\mathcal{O}_{2W}, \mathcal{O}_{2B}, \mathcal{O}_{2G}$  corresponding to the  $Y, W$  and  $Z$  parameters [23] in the generalization of the universal oblique parameters<sup>5</sup>. The coefficients  $\bar{c}_{WB}$  and the combination  $\bar{c}_W + \bar{c}_B$  are related to the  $\hat{S}$  parameter, and we eliminate the former using the identity

$$\mathcal{O}_B = \mathcal{O}_{HB} + \frac{1}{4} \mathcal{O}_{BB} + \frac{1}{4} \mathcal{O}_{WB} .$$

The operators  $\mathcal{O}_{HB}, \mathcal{O}_{BB}$  affect Higgs physics and triple-gauge couplings, as we shall see in the next section. Finally, the  $\hat{T}$  parameter is equivalent to the  $\bar{c}_T$  coefficient. These operators are listed in Table 1.

<sup>5</sup>The  $U, V$  and  $X$  parameters correspond to higher-dimensional operators.

The corrections to the self-energies are then as in (2.1), with  $\hat{S} = \bar{c}_W + \bar{c}_B$  and  $\hat{T} = \bar{c}_T$ . We also have the input observable correction

$$\xi_{G_F} = -2\bar{c}_{LL}^{(3)l},$$

and direct contributions to the output observables,

$$\begin{aligned}\xi_{\Gamma_Z} &= \frac{\Gamma_Z^l}{\Gamma_Z} \xi_{\Gamma_Z^l} + \frac{\Gamma_Z^{\text{had}}}{\Gamma_Z} \xi_{\Gamma_Z^{\text{had}}}, \\ \xi_{\sigma_{\text{had}}^0} &= \xi_{\Gamma_Z^e} + \xi_{\Gamma_Z^{\text{had}}} - 2\xi_{\Gamma_Z}, \\ \xi_{R_l} &= \xi_{\Gamma_Z^{\text{had}}} - \xi_{\Gamma_Z^l}, \\ \xi_{R_q} &= \xi_{\Gamma_Z^q} - \xi_{\Gamma_Z^{\text{had}}}, \\ \xi_{A_{\text{FB}}^{0,f}} &= \xi_{A_e} + \xi_{A_f},\end{aligned}$$

which can be written in terms of shifts to the  $Z$ -fermion couplings,

$$\begin{aligned}\xi_{A_f} &= \frac{4(g_Z^{fL})^2(g_Z^{fR})^2}{(g_Z^{fL})^4 - (g_Z^{fR})^4} \left( \xi_{g_Z^{fL}} - \xi_{g_Z^{fR}} \right), \\ \xi_{\Gamma_Z^f} &= \frac{2(g_Z^{fL})^2}{(g_Z^{fL})^2 + (g_Z^{fR})^2} \xi_{g_Z^{fL}} + \frac{2(g_Z^{fR})^2}{(g_Z^{fL})^2 + (g_Z^{fR})^2} \xi_{g_Z^{fR}},\end{aligned}$$

where

$$\xi_{g_Z^{fL}} = \frac{1}{g_Z^{fL}} \left( T_f^3 \bar{c}_{fL}^{(3)} - \frac{\bar{c}_{fL}}{2} \right), \quad \xi_{g_Z^{fR}} = -\frac{\bar{c}_{fR}}{2g_Z^{fR}},$$

and  $g_Z^f \equiv T_f^3 - Q_f s_{\theta_W}^2$ . Using these expressions and the expansion formalism in a  $\chi^2$  analysis, we obtain 95% CL limits for the operator coefficients.

The left panel of Fig. 2 shows our results for fits to the coefficients  $\bar{c}_{LL}^{(3)l}$ ,  $\bar{c}_T$ ,  $\bar{c}_W + \bar{c}_B$ , together with the coefficient  $\bar{c}_R^e$  that affects the leptonic observables  $\{\Gamma_Z, \sigma_{\text{had}}^0, R_e^0, R_\mu^0, R_\tau^0, A_{\text{FB}}^{0,e}, m_W\}$ . The upper (green) bars indicate the ranges for each of the coefficients varied individually, assuming that the other coefficients vanish, and the lower (red) bars show the ranges for a global fit in which all the coefficients are varied simultaneously. In both fits, the coefficients are all quite compatible with zero, with ranges  $\sim \pm 0.001$  in the single-coefficient analysis, increasing in the global fit up to  $\sim \pm 0.004$  for the coefficient  $\bar{c}_T$  in the multi-coefficient analysis<sup>6</sup>. The legend at the top of the left panel of Fig. 2 translates the ranges of the coefficients into ranges of sensitivity to a large mass scale  $\Lambda$ . We see that all the sensitivities are in the multi-TeV range, including in the global analysis.

The right panel of Fig. 2 shows the effect of including the hadronic observables,  $\{R_b^0, R_c^0, A_{\text{FB}}^{0,b}, A_{\text{FB}}^{0,c}, A_b, A_c\}$ , and the coefficients that contribute directly to them, namely  $\bar{c}_L^q, \bar{c}_L^{(3)q}, \bar{c}_R^u$  and  $\bar{c}_R^d$ . The ranges for the single-variable fits to  $\bar{c}_{LL}^{(3)l}$ ,  $\bar{c}_T$ ,  $\bar{c}_W + \bar{c}_B$  and  $\bar{c}_R^e$  (upper, green lines) are the same as in the left panel, but the horizontal scales are different, as seen immediately by comparing the separations of the vertical black dashed ‘tramlines’. The ranges of these coefficients are altered significantly in the global 8-coefficient fit (lower, red lines) and we see significant tension with the null hypotheses for  $\bar{c}_{LL}^{(3)l}$ ,  $\bar{c}_T$ ,  $\bar{c}_W + \bar{c}_B$  and  $\bar{c}_R^e$ , which reflects the well-known tension

<sup>6</sup>We note that larger marginalized ranges for  $\bar{c}_R^e$  and  $\bar{c}_{LL}^{(3)l}$  are found in [13], warranting further cross-checks.

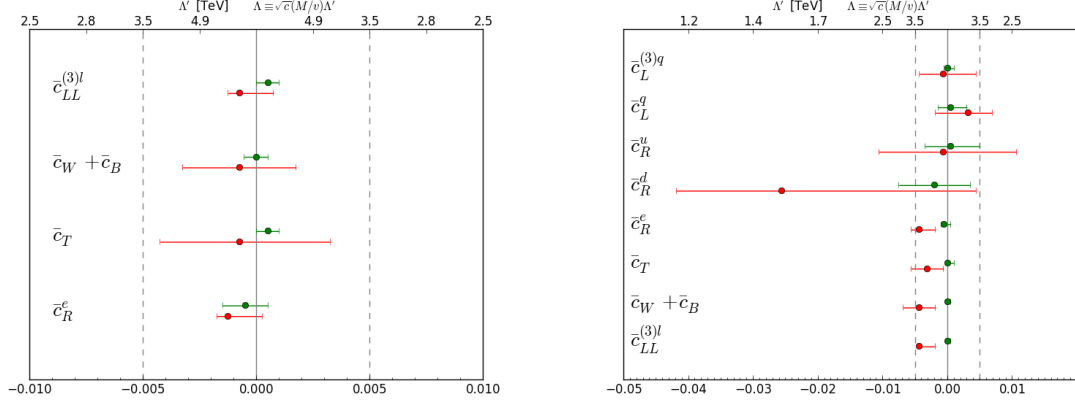


**Figure 2:** The 95% CL ranges found in analyses of the leptonic observables (left panel) and including also the hadronic observables (right panel). In each case, the upper (green) bars denote single-coefficient fits, and the lower (red) bars denote multi-coefficient fits. The upper-axis should be read  $\times \frac{m_W}{v} \sim 1/3$  for  $\bar{c}_W + \bar{c}_B$ .

between the Standard Model and heavy-flavour measurements at the  $Z$  peak. However, values of  $\bar{c}_{LL}^{(3)l}$ ,  $\bar{c}_T$ ,  $\bar{c}_W + \bar{c}_B$  and  $\bar{c}_R^e$  between 0 and -0.01 are favoured, corresponding to  $\Lambda \gtrsim 2.5$  TeV. The ranges of  $\bar{c}_L^q$ ,  $\bar{c}_L^{(3)q}$ ,  $\bar{c}_R^u$  and  $\bar{c}_R^d$  are considerably broader in both fits, particularly in the global 8-coefficient fit, most notably  $\bar{c}_R^u$  and  $\bar{c}_R^d$ , with values of the latter approaching -0.05 being allowed at the 95% CL.

### 3 Triple-Gauge and Higgs Couplings at the LHC

In previous work [14] we used LHC measurements of Higgs signal strengths together with differential distributions in Higgs associated production measurements by ATLAS and D0 to constrain all the dimension-6 operators affecting Higgs physics. The associated production information was vital in eliminating a blind direction, which can also be closed by including TGC measurements. These are most precisely measured by LEP, but it has been recently pointed out that the LEP TGC constraints<sup>7</sup> have a direction of limited sensitivity due to accidental partial cancellations [21]. Meanwhile, TGCs have been analysed at 8 TeV at the LHC by both the CMS and ATLAS experiments [19, 20], and here we study their potential to complement Higgs physics in constraining a complete set of dimension-6 operators.

Operator	Coefficient	LHC Constraints	
		Individual	Marginalized
$\mathcal{O}_W = \frac{ig}{2} \left( H^\dagger \sigma^a \overleftrightarrow{D}^\mu H \right) D^\nu W_{\mu\nu}^a$ $\mathcal{O}_B = \frac{ig'}{2} \left( H^\dagger \overleftrightarrow{D}^\mu H \right) \partial^\nu B_{\mu\nu}$	$\frac{m_W^2}{\Lambda^2} (c_W - c_B)$	(-0.022, 0.004)	(-0.035, 0.005)
$\mathcal{O}_{HW} = ig(D^\mu H)^\dagger \sigma^a (D^\nu H) W_{\mu\nu}^a$	$\frac{m_W^2}{\Lambda^2} c_{HW}$	(-0.042, 0.008)	(-0.035, 0.015)
$\mathcal{O}_{HB} = ig'(D^\mu H)^\dagger (D^\nu H) B_{\mu\nu}$	$\frac{m_W^2}{\Lambda^2} c_{HB}$	(-0.053, 0.044)	(-0.045, 0.075)
$\mathcal{O}_{3W} = \frac{1}{3!} g \epsilon_{abc} W_\mu^{a\nu} W_\nu^b W^c{}_{\rho\mu}$	$\frac{m_W^2}{\Lambda^2} c_{3W}$	(-0.083, 0.045)	(-0.083, 0.045)
$\mathcal{O}_g = g_s^2  H ^2 G_{\mu\nu}^A G^{A\mu\nu}$	$\frac{m_W^2}{\Lambda^2} c_g$	$(0, 3.0) \times 10^{-5}$	$(-3.2, 1.1) \times 10^{-4}$
$\mathcal{O}_\gamma = g'^2  H ^2 B_{\mu\nu} B^{\mu\nu}$	$\frac{m_W^2}{\Lambda^2} c_\gamma$	$(-4.0, 2.3) \times 10^{-4}$	$(-11, 2.2) \times 10^{-4}$
$\mathcal{O}_H = \frac{1}{2} (\partial^\mu  H ^2)^2$	$\frac{v^2}{\Lambda^2} c_H$	(-, -)	(-, -)
$\mathcal{O}_f = y_f  H ^2 \bar{F}_L H^{(c)} f_R + \text{h.c.}$	$\frac{v^2}{\Lambda^2} c_f$	(-, -)	(-, -)

**Table 2:** List of operators in our basis entering in LHC Higgs (including  $D0$  associated production) and TGC physics, together with 95% CL bounds when individual coefficients are switched on one at a time, and marginalized in a simultaneous fit.

### 3.1 TGC Constraints on Dimension-6 Operator Coefficients

The operators affecting Higgs physics and TGCs in the basis we adopt are listed in Table 2, with the Lagrangian given by

$$\begin{aligned}
\mathcal{L}_{\text{dim-6}} \supset & \frac{\bar{c}_W}{m_W^2} \mathcal{O}_W + \frac{\bar{c}_B}{m_W^2} \mathcal{O}_B + \frac{\bar{c}_{HW}}{m_W^2} \mathcal{O}_{HW} + \frac{\bar{c}_{HB}}{m_W^2} \mathcal{O}_{HB} + \frac{\bar{c}_\gamma}{m_W^2} \mathcal{O}_\gamma + \frac{\bar{c}_g}{m_W^2} \mathcal{O}_g \\
& + \frac{\bar{c}_{3W}}{m_W^2} \mathcal{O}_{3W} + \sum_{f=l,b,\tau} \frac{\bar{c}_f}{v^2} \mathcal{O}_f + \frac{\bar{c}_H}{v^2} \mathcal{O}_H + \frac{\bar{c}_6}{v^2} \mathcal{O}_6.
\end{aligned}$$

The constraint at the per-mille level on the combination  $\bar{c}_W + \bar{c}_B$  obtained in the previous Section allows us to set  $\bar{c}_B = -\bar{c}_W$  (or equivalently to constrain the direction  $\bar{c}_W - \bar{c}_B$ ). Ignoring the unconstrained operator  $\mathcal{O}_6$  that affects the Higgs self-couplings and (for simplicity) setting  $\bar{c}_b = \bar{c}_\tau \equiv \bar{c}_d$  then reduces the number of independent coefficients to nine. The coefficients  $\bar{c}_W, \bar{c}_{HW}, \bar{c}_{HB}$  and  $\bar{c}_{3W}$  affect TGCs, with  $\bar{c}_{3W}$  being limited only by TGC measurements, since it does not affect Higgs physics.

We calculate the TGCs in the presence of dimension-6 operators using the `FeynRules` implementation of [34] in `MadGraph v2.1.2` [35], interfaced with `Pythia` [36] and `Delphes` [37]. In the case of ATLAS, we implement the analysis given in [20]. This requires events that pass the selection cuts to have exactly 2 opposite-sign leptons with no jets,  $p_T > 25(20)$  GeV for leading (sub-leading) leptons,  $m_{ll} > 15(10)$  GeV and  $E_T^{\text{miss}} > 45(15)$  GeV for same-flavour (different-flavour) lepton pairs, as well as  $|m_{ll} - m_Z| > 15$  GeV for the same-flavour case. Similarly, following [19], for the CMS cuts we require 2 opposite-sign leptons with  $p_T > 20$  GeV, total lepton  $p_T > 45$  GeV and  $75 \text{ GeV} < m_{ll} < 105$  GeV,  $E_T^{\text{miss}} > 37(20)$  GeV and  $m_{ll} > 20(12)$  GeV for same-flavour (opposite-flavour) pairs, and no jets with  $|\eta| < 5, E_T > 30$  GeV.

<sup>7</sup>See also [30] for a recent discussion on the use of TGC observables as reported by LEP for constraining dimension-6 operators in different bases.

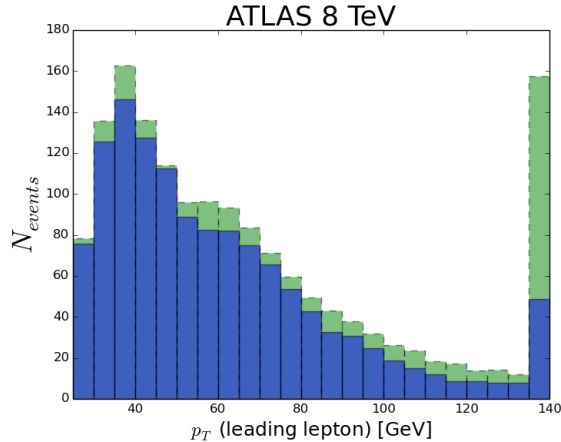


**Figure 3:** *The same-flavour  $p_T$  distribution of the leading lepton after the TGC analysis cuts for ATLAS at 8 TeV. The Standard Model distribution is shown in blue with solid lines, and the effect of  $\bar{c}_{HW} = 0.1$  is superimposed in green with dashed lines.*

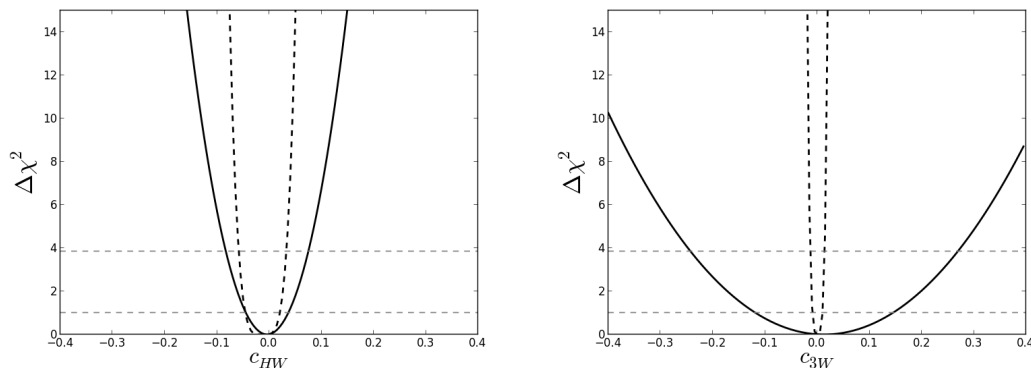


**Figure 4:** *Comparisons between the  $\chi^2$  functions from fits to the same-flavour ATLAS distribution including only linear (solid lines) and also quadratic (dashed lines) dependences on the dimension-6 coefficients  $\bar{c}_{HW}$  (left panel) and  $\bar{c}_{3W}$  (right panel).*

The resulting  $p_T$  distribution of the leading lepton for the ATLAS 8 TeV analysis is shown in Fig. 3 including  $\bar{c}_{HW} = 0.1$  as well as the Standard Model contribution<sup>8</sup>. We focus on the number of events in the last (overflow) bin, since this has the highest signal-to-background ratio and grows rapidly as a function of this and the other dimension-6 coefficients<sup>9</sup>. We prefer to keep only the linear dependences on the dimension-6 coefficients, considering that it is not consistent to keep terms that are quadratic in the dimension-6 coefficients if one does not have reason to expect that the coefficients of dimension-8 operators would be suppressed. As an example, we note that the signal-strength dependence of the overflow bin on  $\bar{c}_{HW}$  for the

<sup>8</sup>The applicability of the effective field theory approach to this TGC analysis is discussed in the Appendix.

<sup>9</sup>The validity of the effective field theory at such high  $p_T$  may be restricted only to certain models [38], but the range of validity will increase as the current precision of LHC TGC measurements is improved.

ATLAS 8-TeV same-flavour distribution is found to be

$$\mu_{\text{last-bin}}^{\text{ATLAS8}} = 1 + 3.45\bar{c}_{HW} + 234\bar{c}_{HW}^2,$$

and we keep only the linear term in our global fits. The constraints obtained using this linear (quadratic) dependence on the dimension-6 coefficients are plotted as solid (dashed) lines in Fig. 4. The left panel is for  $\bar{c}_{HW}$ , and right panel is for  $\bar{c}_{3W}$ . When deriving constraints we use the background and Standard Model signal Monte-Carlo (MC) distributions of the leading lepton  $p_T$  provided by the experiments, and marginalize over the MC error. This is given along with the observed number of events and their errors in [20] for ATLAS and [19] for CMS. We see that the quadratic and linear fits for  $\bar{c}_{HW}$  are quite similar, whereas the constraint from the (preferred) linear fit for  $\bar{c}_{3W}$  is significantly weaker than that from the (deprecated) quadratic fit.

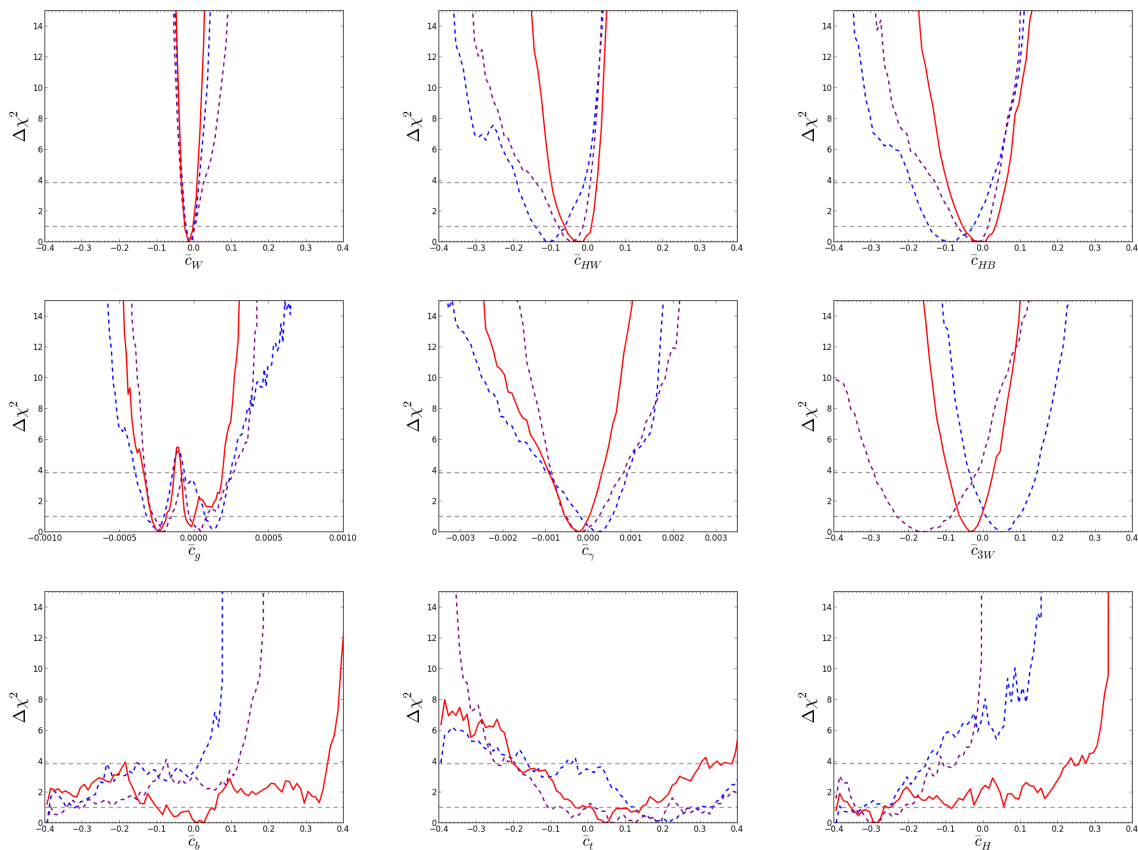


**Figure 5:** Comparisons of the constraints on the dimension-6 coefficients  $\bar{c}_W$ ,  $\bar{c}_{HW}$  and  $\bar{c}_{HB}$  (top row),  $\bar{c}_g$ ,  $\bar{c}_\gamma$  and  $\bar{c}_{3W}$  (middle row), and  $\bar{c}_b$ ,  $\bar{c}_t$  and  $\bar{c}_H$  (bottom row) provided by the LHC signal-strength data together with the ATLAS 8-TeV (purple lines), the CMS 7- and 8-TeV TGC measurements (blue lines) and their combination (red lines).

For the full global fit we use the same-flavour and different-flavour distributions for ATLAS at 8 TeV and the CMS 7 and 8 TeV data. In Fig. 5 we compare the constraints from the combination of the ATLAS and CMS TGC measurements with the LHC Higgs signal-strength data on each of the dimension-6 coefficients  $\bar{c}_W$ ,  $\bar{c}_{HW}$  and  $\bar{c}_{HB}$  (top row),  $\bar{c}_g$ ,  $\bar{c}_\gamma$  and  $\bar{c}_{3W}$

(middle row), and  $\bar{c}_b$ ,  $\bar{c}_t$  and  $\bar{c}_H$  (bottom row)<sup>10</sup> The purple line represents the combination of LHC signal-strength constraints with the ATLAS 8-TeV TGC measurements, the blue line the combination of CMS 7- and 8-TeV constraints, and the red line uses all the sets of LHC TGC constraints. We use the signal-strength information on the  $W^+W^{-(*)}$ ,  $ZZ^{(*)}$ ,  $\gamma\gamma$ ,  $Z\gamma$ , and  $\tau^+\tau^-$  final states, whose likelihoods are obtained as explained in [14]. We observe that the constraints on the coefficient  $\bar{c}_{3W}$ , which only affects TGCs, is at the same level as some of the other coefficients whose operators also affect Higgs physics.

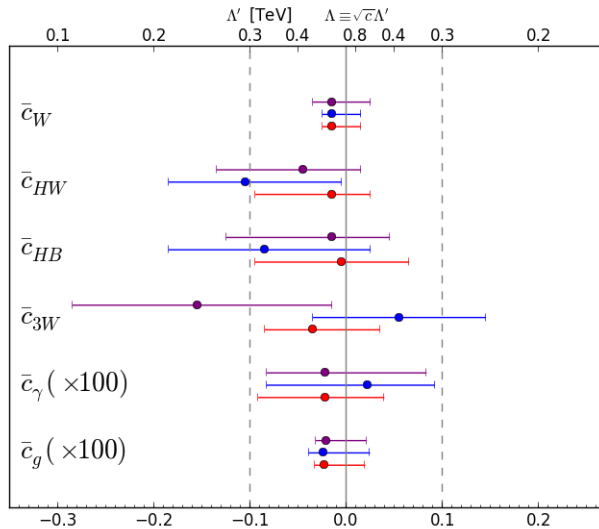


**Figure 6:** The marginalised 95% CL ranges for the dimension-6 operator coefficients obtained by combining the LHC signal-strength data with the ATLAS 8-TeV TGC data (purple bars), the CMS 7- and 8-TeV TGC measurements (blue bars), and their combination (red bars). Note that  $\bar{c}_{\gamma,g}$  are shown  $\times 100$ , so for these coefficients the upper axis should therefore be read  $\times 10$ .

The results in Fig. 5 are summarised in the marginalised 95% CL ranges displayed in Fig. 6. Again, the LHC signal-strength data are always included, in combination with the ATLAS 8-TeV data (purple bars), the CMS 7- and 8-TeV data (blue bars) and all the LHC TGC data (red bars). As already mentioned, the LHC TGC data enables a competitive model-independent bound on the coefficient  $\bar{c}_{3W}$ .

### 3.2 Inclusion of Higgs Associated Production Constraints

We now include in our analysis the constraints from the kinematics of associated Higgs production, following the analysis of [14]<sup>11</sup>. Fig. 7 displays the marginalised  $\chi^2$  distributions for each of the dimension-6 coefficients  $\bar{c}_W$ ,  $\bar{c}_{HW}$  and  $\bar{c}_{HB}$  (top row),  $\bar{c}_g$ ,  $\bar{c}_\gamma$  and  $\bar{c}_{3W}$  (middle row),

<sup>10</sup>We note that the constraints on the last three operators are relatively weak, but include them for information.

<sup>11</sup>The applicability of the effective field theory approach to this associated production analysis is discussed in the Appendix.

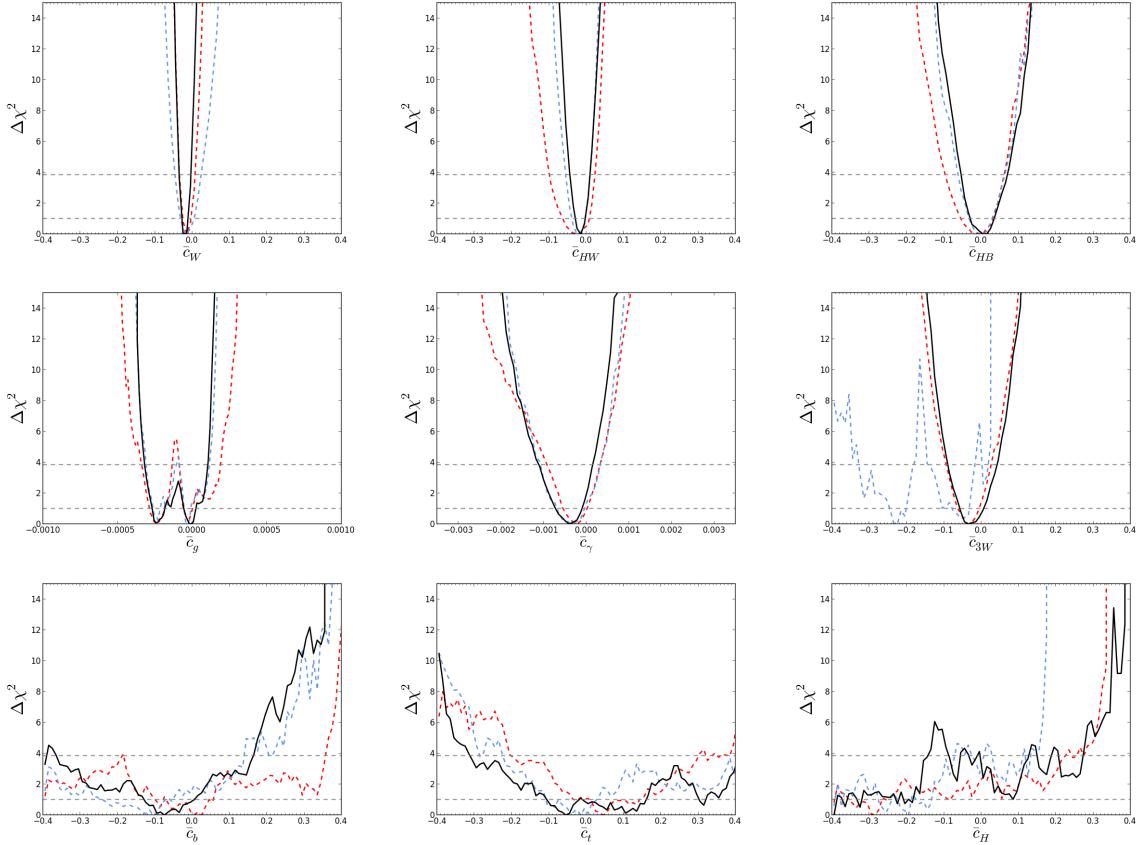


**Figure 7:** The marginalised  $\chi^2$  distributions for each of the dimension-6 coefficients  $\bar{c}_W$ ,  $\bar{c}_{HW}$  and  $\bar{c}_{HB}$  (top row),  $\bar{c}_g$ ,  $\bar{c}_\gamma$  and  $\bar{c}_{3W}$  (middle row), and  $\bar{c}_b$ ,  $\bar{c}_t$  and  $\bar{c}_H$  (bottom row), including the signal strengths measured at the LHC and the constraints from the kinematic distributions for associated  $H + V$  production measured by ATLAS and D0 (dashed blue lines), the signal strengths and the LHC TGC measurements (red lines), and all the constraints (black lines).

and  $\bar{c}_b$ ,  $\bar{c}_t$  and  $\bar{c}_H$  (bottom row)<sup>12</sup>. In each panel, the dashed blue line includes the Higgs signal strengths measured at the LHC and the constraints from the kinematic distributions for associated  $H + V$  production measured by ATLAS and D0, whereas the solid red line includes the signal strengths and the LHC TGC measurements. The solid black lines include all the constraints: the signal strengths, the kinematic distributions and the TGCs measured at the LHC. We see that the LHC TGC measurements are the strongest for  $\bar{c}_W$  and  $\bar{c}_{3W}$ : in particular, they are necessary to obtain any meaningful constraint on  $\bar{c}_{3W}$ , which is not constrained at all by Higgs physics alone. On the other hand, the Higgs constraints are more important for  $\bar{c}_{HW}$ ,  $\bar{c}_{HB}$  and  $\bar{c}_g$ , whereas the TGC and Higgs constraints are of comparable importance for the other coefficients.

The results of our fits are summarised in Fig. 8. The individual 95% CL constraints obtained by switching one coefficient on at a time are shown as green bars. The other lines are the marginalised 95% ranges obtained using the LHC signal-strength data in combination with the

<sup>12</sup>We note again that the constraints on the last three operators are relatively weak, but include them for information.

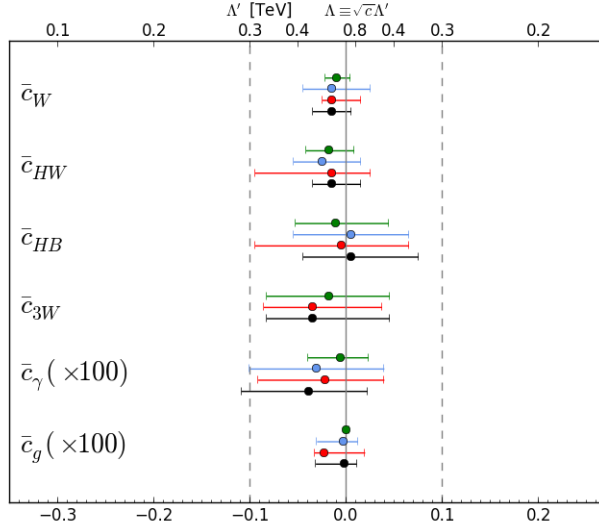


**Figure 8:** The 95% CL constraints obtained for single-coefficient fits (green bars), and the marginalised 95% ranges for the LHC signal-strength data combined with the kinematic distributions for associated  $H + V$  production measured by ATLAS and D0 (blue bars), combined with the LHC TGC data (red lines), and the global combination with both the associated production and TGC data (black bars). Note that  $\bar{c}_{\gamma,g}$  are shown  $\times 100$ , so for these coefficients the upper axis should therefore be read  $\times 10$ .

kinematic distributions for associated  $H + V$  production measured by ATLAS and D0 (blue bars), in combination with the LHC TGC data (red lines), and in combination with both the associated production and TGC data (black bars). We see again that the LHC TGC constraints are the most important for  $\bar{c}_W$  and  $\bar{c}_{3W}$ , whereas the Higgs constraints are more important for  $\bar{c}_{HW}$ ,  $\bar{c}_{HB}$  and  $\bar{c}_g$ . Our numerical results for the 95% CL ranges for these coefficients are shown alongside the operator definitions in Table 2.

## 4 Application to the Two-Higgs Doublet Model

We now discuss an example of the application of our constraints to a specific ultra-violet (UV) completion of the effective field theory. The case of a singlet scalar and stops contributing to dimension-6 operators was recently considered in [32]. Here we briefly look at applying our constraints to the 2HDM scenario, which is worth further investigation [33].

In a large range of models, the only coupling of the Higgs to massive vector bosons has the following Lorentz structure

$$hW_{\mu\nu}W^{\mu\nu}. \quad (4.1)$$

The translation between this Higgs anomalous coupling and the operators is given in [34] (see also [39]). The following constraints

$$\bar{c}_{HW} = -\bar{c}_W, \quad \bar{c}_{HB} = -\bar{c}_B \quad (4.2)$$

are then satisfied at the UV scale. We recall from Section 2 that, in addition, the EWPTs

impose the constraint  $\bar{c}_W \simeq -\bar{c}_B$ , implying that, to a good approximation

$$\bar{c}_W = -\bar{c}_B = -\bar{c}_{HW} = \bar{c}_{HB}, \quad (4.3)$$

with corrections due to renormalization-group running effects that are negligible compared to the precision of the current LHC constraints. Moreover, in the 2DHM one also finds generically that  $\bar{c}_{3W}$  is suppressed [33]

$$\bar{c}_{3W} \sim \mathcal{O}(0.1)g^2\bar{c}_{HW}, \quad (4.4)$$

so that it can be an order of magnitude smaller. In our application to the 2HDM we set it to zero, as well as using the constraints (4.3).

Examples of models in this class include a general two-Higgs doublet model (2HDM) [33], supersymmetry with electroweakino/sfermion loops [40], and the exchange of a radion/dilaton particle [39]. In the former two models these operators are generated at loop level, whereas in the third case the operators appear at tree-level through the exchange of the radion/dilaton particle. In the loop-induced cases, the validity of the effective theory is typically  $\sqrt{\hat{s}} \sim 2M$ , where  $M$  is the mass scale of the heavy states.

Fig. 9 shows the  $\chi^2$  distributions we find in a global fit to the three independent dimension-6 coefficients of the 2HDM,  $\bar{c}_W$ ,  $\bar{c}_g$  and  $\bar{c}_\gamma$  obtained under these assumptions. These distributions have been obtained including all the constraints from the signal strengths measured at the LHC, the constraints from the kinematic distributions for associated  $H + V$  production measured by ATLAS and D0, and the LHC TGC measurements. We find the following 95% CL ranges

$$\begin{aligned} \bar{c}_W &\in -(0.02, 0.0004) \\ \bar{c}_g &\in -(0.00004, 0.000003) \\ \bar{c}_\gamma &\in -(0.0006, -0.00003) \end{aligned} \quad (4.5)$$

in this particular class of models.

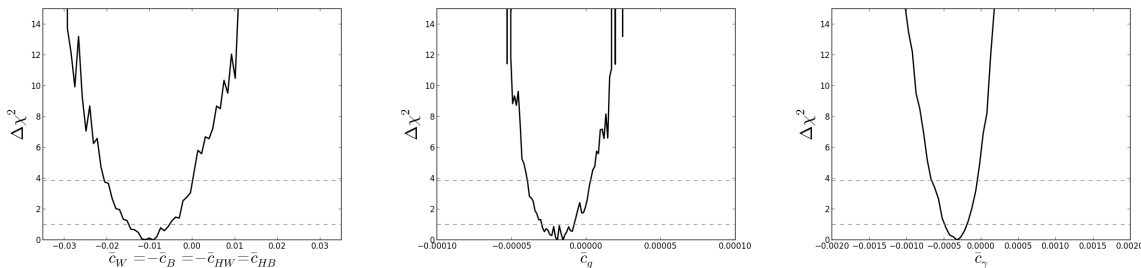


**Figure 9:** The marginalised  $\chi^2$  distributions for the coefficients  $\bar{c}_W = -\bar{c}_B = -\bar{c}_{HW} = \bar{c}_{HB}$ ,  $\bar{c}_g$ , and  $\bar{c}_\gamma$  of the three independent dimension-6 operators in the 2HDM under the assumptions stated in the text.

## 5 Conclusions

The main lesson learned from Run I of the LHC is that, to a first approximation, we seem to have a Standard Model-like Higgs sector. Taken together with the fact that there is currently no clear evidence for any new physics beyond the Standard Model, it is natural to consider

the Standard Model in its complete effective theory formulation. Such a (relatively) model-independent framework parameterises all the possible ways in which decoupled new physics may affect measurements at different experiments in a correlated and motivated way.

We have analysed in this paper the constraints imposed on the coefficients of dimension-6 operator extensions of the Standard Model by EWPTs and LHC data. We first analysed the EWPTs using the expansion formalism of [27], which is particularly appropriate for models where the dominant corrections to the Standard Model predictions are not necessarily present only in the vector-boson self-energies, as is the case for general dimension-6 extensions of the Standard Model. We confirm previous findings that the EWPTs provide particularly important constraints on some of the operator coefficients, as shown in Fig. 2 and Table 1.

We then analysed the TGC data now available from ATLAS at 8 TeV and from CMS at 7 and 8 TeV. We find that the most important aspects of the data are the highest-energy (overflow) bins in the lepton  $p_T$  distributions, as illustrated in Fig. 3, and use these together with Higgs signal strength measurements to obtain constraints on a set of nine operator coefficients, as shown in Figs. 5 and 6. We then combined these LHC TGC constraints with the constraints provided by measurements of the kinematics of Higgs production in association with massive vector bosons at the Tevatron and the LHC, obtaining the results shown in Figs. 7 and 8 and Table 2. As seen there, we find that completing the Higgs signal strengths constraints on dimension-6 operators using the LHC TGCs provide the strongest LHC constraints on some of the coefficients, whereas the Higgs differential distributions in associated production are more important for some others, with both making important contributions in some cases. In particular, we obtain the first bounds on the coefficient  $\bar{c}_{3W}$  for a complete basis in the effective Standard Model. It is only by combining the TGC and Higgs constraints that one can obtain a complete picture of the possible ranges of the dimension-6 operator coefficients after LHC Run 1.

It is to be expected that Run 2 of the LHC will provide important improvements in the sensitivity of LHC probes of possible dimension-6 operators. These improvements will come not only from the greater statistics, but also from the greater kinematic range that will strengthen the power of the associated Higgs production kinematics and the TGC constraints, in particular. At the moment we know that the Standard Model is very effective: LHC Run 2 data will give us a better idea just how effective it is, and perhaps provide some pointers to the nature of the new physics that surely lies beyond it at higher energies.

## Acknowledgements

We thank Francesco Riva for useful conversations and Maxime Gouzevitch and Alexander Savin for helpful information about the CMS TGC distributions. The work of JE was supported partly by the London Centre for Terauniverse Studies (LCTS), using funding from the European Research Council via the Advanced Investigator Grant 26732, and partly by the STFC Grant ST/J002798/1. The work of VS was supported by the STFC Grant ST/J000477/1. The work of TY was supported by a Graduate Teaching Assistantship from King's College London.

# Appendix: Kinematics and the Validity of the Effective Field Theory

We use in Section 3 triple-gauge couplings and information on kinematic distributions in Higgs production in association with a vector boson production constraints, finding that typical 95% CL constraints on the dimension-6 coefficients are  $\mathcal{O}(10^{-1} - 10^{-2})$ . For example, for the operator  $\bar{c}_W$  our limits are

$$\bar{c}_W \in (-0.022, 0.004) \text{ [one-by-one]} \text{ and } (-0.035, 0.005) \text{ [global]}. \quad (5.1)$$

Recalling the definition of the barred coefficients in Eq. 2.3, one can interpret these limits in terms of new physics at scale  $\Lambda$  coupled to the SM with strength  $g_{\text{NP}}$ ,

$$\frac{\bar{c}_W}{m_W^2} = \frac{g_{\text{NP}}^2}{\Lambda^2}, \quad (5.2)$$

upto a factor  $g$  from the conventional definition of  $\mathcal{O}_W$ . The value of  $\Lambda$  corresponding to a value of  $\bar{c}_W$  can be read off the upper x-axis in Fig. 8 assuming  $g_{\text{NP}}^2 = 1$ , where we see that the marginalized range for  $\bar{c}_W$  corresponds to  $\Lambda \sim 400 - 800$  GeV. However  $g_{\text{NP}}$  may vary to be less than 1 in weakly-coupled scenarios, in which case the new physics scale is lowered, or up to  $4\pi$  for strongly-coupled new physics, which raises  $\Lambda$ . In general we have

$$\Lambda_{\bar{c}_W} \simeq \left( \frac{g_{\text{NP}}}{4\pi} \right) 10 \text{ TeV}. \quad (5.3)$$

The question can be asked whether the effective Standard Model approach is justified.

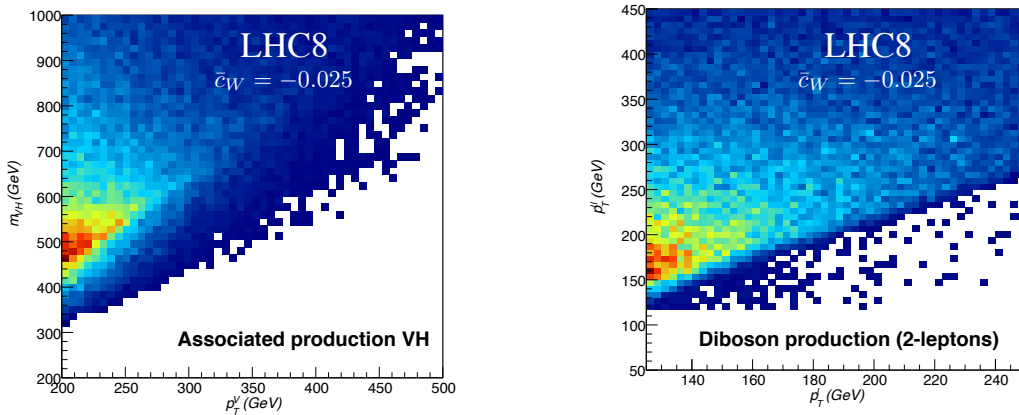


**Figure 10:** (Left) The kinematic distribution in the vector boson  $p_T^V$  vs  $m_{VH}$  plane for associated Higgs production at the LHC that would be induced by  $\bar{c}_W = -0.025$ . (Right) The kinematic distribution in the leading lepton  $p_T$  vs  $p_T^{\ell\ell}$  plane for diboson production at the LHC that would be induced by  $\bar{c}_W = -0.025$ .

In this Appendix we address this question by considering the region where the most sensitivity is obtained, i.e., the last bin. First of all, it is important to note that the last bin is an overflow bin, containing all the events with  $p_T$  above a specified cut. For example, in the TGC analysis shown in Fig. 3 the last bin corresponds to  $p_T > 135$  GeV.

For a given value of  $\Lambda$ , one expects the effective theory to break down at parton energies  $\sqrt{\hat{s}} \simeq \Lambda$ , namely  $m_{VV}$  and  $m_{VH}$  in the diboson and VH production respectively. To illustrate this point, in Fig. 10 we show the kinematic distribution that would be induced by  $\bar{c}_W = -0.025$  (our most conservative limit in  $\bar{c}_W$ ) in the plane defined by the transverse momentum of the vector boson,  $p_T^V$ , and the invariant mass,  $m_{VH}$ , for associated Higgs production at the LHC in the 2-lepton channel. This plot corresponds to the last bin of the distribution, which has a cut  $p_T^V > 200$  GeV. We see that in this bin typically  $p_T^V \lesssim 250$  GeV, i.e., there is not a large spread of events at large values of the distribution, and  $\sqrt{\hat{s}} = m_{VH} \lesssim 550$  GeV.

One can perform a similar analysis in the di-boson production case. For comparison, we show in the right panel of Fig. 10 the  $p_T$  distribution of the leading lepton in the  $pp \rightarrow W^+W^- \rightarrow 2\ell + \cancel{E}_T$  production at LHC8 versus the transverse mass distribution of the two vector bosons,  $p_T^{\ell\ell}$ . For comparison with Fig. 3, we infer that the overflow bin of  $p_T > 135$  GeV extends to about 160 GeV, and is correlated with  $p_T^{\ell\ell} < 250$  GeV.

Thus, in both the associated production and TGC cases, for  $g_{NP} = \mathcal{O}(1)$ , equation (5.3) reassures us that the most important regions of the kinematical distributions are well within the ranges where one may expect the effective field theory to be a good enough approximation for our purposes.

## References

- [1] G. Aad *et al.* [ATLAS Collaboration], Phys. Lett. B **716** (2012) 1 [arXiv:1207.7214 [hep-ex]]; S. Chatrchyan *et al.* [CMS Collaboration], Phys. Lett. B **716** (2012) 30 [arXiv:1207.7235 [hep-ex]].
- [2] M. Baak, M. Goebel, J. Haller, A. Hoecker, D. Ludwig, K. Moenig, M. Schott and J. Stelzer, Eur. Phys. J. C **72** (2012) 2003 [arXiv:1107.0975 [hep-ph]]. D. Carmi, A. Falkowski, E. Kuflik and T. Volanski, arXiv:1202.3144 [hep-ph]; A. Azatov, R. Contino and J. Galloway, JHEP **1204** (2012) 127 [hep-ph/1202.3415]. J.R. Espinosa, C. Grojean, M. Muhlleitner and M. Trott, arXiv:1202.3697 [hep-ph]; P. P. Giardino, K. Kannike, M. Raidal and A. Strumia, arXiv:1203.4254 [hep-ph]; T. Li, X. Wan, Y. Wang and S. Zhu, arXiv:1203.5083 [hep-ph]; M. Rauch, arXiv:1203.6826 [hep-ph]; J. Ellis and T. You, JHEP **1206** (2012) 140, [arXiv:1204.0464 [hep-ph]]; A. Azatov, R. Contino, D. Del Re, J. Galloway, M. Grassi and S. Rahatlou, arXiv:1204.4817 [hep-ph]; M. Klute, R. Lafaye, T. Plehn, M. Rauch and D. Zerwas, arXiv:1205.2699 [hep-ph]; L. Wang and X.-F. Han, Phys. Rev. D **86** (2012) 095007, [arXiv:1206.1673 [hep-ph]]; D. Carmi, A. Falkowski, E. Kuflik and T. Volansky, arXiv:1206.4201 [hep-ph]; M. J. Dolan, C. Englert and M. Spannowsky, arXiv:1206.5001 [hep-ph]; J. Chang, K. Cheung, P. Tseng and T. Yuan, arXiv:1206.5853 [hep-ph]; S. Chang, C. A. Newby, N. Raj and C. Wanotayaroj, arXiv:1207.0493 [hep-ph]; I. Low, J. Lykken and G. Shaughnessy, arXiv:1207.1093 [hep-ph]; J. Ellis and T. You, JHEP **1209**, 123 (2012) [arXiv:1207.1693 [hep-ph]]. P. P. Giardino, K. Kannike, M. Raidal and A. Strumia, arXiv:1207.1347 [hep-ph]; M. Montull and F. Riva, arXiv:1207.1716 [hep-ph]; J. R. Espinosa, C. Grojean, M. Muhlleitner and M. Trott, arXiv:1207.1717 [hep-ph]; D. Carmi, A. Falkowski, E. Kuflik, T. Volansky and J. Zupan, arXiv:1207.1718 [hep-ph]; S. Banerjee, S. Mukhopadhyay and B. Mukhopadhyaya, JHEP **10** (2012) 062, [arXiv:1207.3588 [hep-ph]]; F. Bonner, T. Ota, M. Rauch and W. Winter, arXiv:1207.4599 [hep-ph]; T. Plehn and M. Rauch, arXiv:1207.6108 [hep-ph]; A. Djouadi, arXiv:1208.3436 [hep-ph]; B. Batell, S. Gori and L. T. Wang, arXiv:1209.6832 [hep-ph];

- G. Moreau, Phys. Rev. D **87** (2013) 015027, [arXiv:1210.3977 [hep-ph]]; G. Cacciapaglia, A. Deandrea, G. D. La Rochelle and J-B. Flament, arXiv:1210.8120 [hep-ph]; E. Masso and V. Sanz, arXiv:1211.1320 [hep-ph]; R. Tito D’Agnolo, E. Kuflik and M. Zanetti, arXiv:1212.1165 [hep-ph]; A. Azatov and J. Galloway, arXiv:1212.1380 [hep-ph]; G. Bhattacharyya, D. Das and P.B. Pal, Phys. Rev. D **87** (2013) 011702, [arXiv:1212.4651 [hep-ph]]; D. Choudhury, R. Islam, A. Kundu and B. Mukhopadhyaya, arXiv:1212.4652 [hep-ph]; R. S. Gupta, M. Montull and F. Riva, arXiv:1212.5240 [hep-ph]; G. Belanger, B. Dumont, U. Ellwanger, J. F. Gunion and S. Kraml, arXiv:1212.5244 [hep-ph]; K. Cheung, J. S. Lee and P-Y. Tseng, arXiv:1302.3794 [hep-ph]. A. Falkowski, F. Riva and A. Urbano, arXiv:1303.1812 [hep-ph], P. P. Giardino, K. Kannike, I. Masina, M. Raidal and A. Strumia, arXiv:1303.3570 [hep-ph]. J. Ellis and T. You, JHEP **1306** (2013) 103 [arXiv:1303.3879 [hep-ph]], J. Bernon, B. Dumont and S. Kraml, Phys. Rev. D **90** (2014) 7, 071301 [arXiv:1409.1588 [hep-ph]].
- [3] T. Appelquist and J. Carazzone, Phys. Rev. D **11** (1975) 285
- [4] W. Buchmuller and D. Wyler, Nucl. Phys. B **268** (1986) 621.
- [5] H. D. Politzer, Nucl. Phys. B **172** (1980) 349; H. Kluberg-Stern and J. B. Zuber, Phys. Rev. D **12** (1975) 3159; C. Grosse-Knetter, Phys. Rev. D **49** (1994) 6709 [hep-ph/9306321]; C. Arzt, Phys. Lett. B **342** (1995) 189 [hep-ph/9304230]; H. Simma, Z. Phys. C **61** (1994) 67 [hep-ph/9307274]; J. Wudka, Int. J. Mod. Phys. A **9** (1994) 2301 [hep-ph/9406205].
- [6] B. Grzadkowski, M. Iskrzynski, M. Misiak and J. Rosiek, JHEP **1010**, 085 (2010) [arXiv:1008.4884 [hep-ph]].
- [7] K. Hagiwara, S. Ishihara, R. Szalapski and D. Zeppenfeld, Phys. Rev. D **48**, 2182 (1993). K. Hagiwara, R. Szalapski and D. Zeppenfeld, Phys. Lett. B **318**, 155 (1993) [hep-ph/9308347].
- [8] F. Bonnet, M. B. Gavela, T. Ota and W. Winter, Phys. Rev. D **85** (2012) 035016 [arXiv:1105.5140 [hep-ph]]. T. Corbett, O. J. P. Eboli, J. Gonzalez-Fraile and M. C. Gonzalez-Garcia, arXiv:1207.1344 [hep-ph]. R. Contino, M. Ghezzi, C. Grojean, M. Muhlleitner and M. Spira, JHEP **1307** (2013) 035 [arXiv:1303.3876 [hep-ph]]. W. -F. Chang, W. -P. Pan and F. Xu, Phys. Rev. D **88** (2013) 3, 033004 [arXiv:1303.7035 [hep-ph]]. . Corbett, O. J. P. boli, J. Gonzalez-Fraile and M. C. Gonzalez-Garcia, Phys. Rev. Lett. **111** (2013) 1, 011801 [arXiv:1304.1151 [hep-ph]]. A. Hayreter and G. Valencia, Phys. Rev. D **88** (2013) 034033 [arXiv:1304.6976 [hep-ph]]. H. Mebane, N. Greiner, C. Zhang and S. Willenbrock, Phys. Rev. D **88**, no. 1, 015028 (2013) [arXiv:1306.3380 [hep-ph]]. M. B. Einhorn and J. Wudka, Nucl. Phys. B **876** (2013) 556 [arXiv:1307.0478 [hep-ph]]. J. Elias-Miro, J. R. Espinosa, E. Masso and A. Pomarol, JHEP **1311** (2013) 066 [arXiv:1308.1879 [hep-ph]]. S. Banerjee, S. Mukhopadhyay and B. Mukhopadhyaya, Phys. Rev. D **89** (2014) 053010 [arXiv:1308.4860 [hep-ph]]. E. Boos, V. Bunichev, M. Dubinin and Y. Kurihara, Phys. Rev. D **89** (2014) 035001 [arXiv:1309.5410 [hep-ph]]. B. Gripaios and D. Sutherland, Phys. Rev. D **89** (2014) 076004 [arXiv:1309.7822 [hep-ph]]. C. -Y. Chen, S. Dawson and C. Zhang, Phys. Rev. D **89**, 015016 (2014) [arXiv:1311.3107 [hep-ph]]. M. Dahiya, S. Dutta and R. Islam, arXiv:1311.4523 [hep-ph]. C. Grojean, E. Salvioni, M. Schlaffer and A. Weiler, JHEP **1405** (2014) 022 [arXiv:1312.3317 [hep-ph], arXiv:1312.3317]. J. Bramante, A. Delgado and A. Martin,

- Phys. Rev. D **89** (2014) 093006 [arXiv:1402.5985 [hep-ph]]. J. S. Gainer, J. Lykken, K. T. Matchev, S. Mrenna and M. Park, arXiv:1403.4951 [hep-ph]. S. Bar-Shalom, A. Soni and J. Wudka, arXiv:1405.2924 [hep-ph]. G. Amar, S. Banerjee, S. von Buddenbrock, A. S. Cornell, T. Mandal, B. Mellado and B. Mukhopadhyaya, arXiv:1405.3957 [hep-ph]. A. Azatov, C. Grojean, A. Paul and E. Salvioni, arXiv:1406.6338 [hep-ph]. E. Masso, arXiv:1406.6376 [hep-ph]. R. Alonso, E. E. Jenkins and A. V. Manohar, arXiv:1409.0868 [hep-ph]. R. M. Godbole, D. J. Miller, K. A. Mohan and C. D. White, arXiv:1409.5449 [hep-ph]. F. Goertz, A. Papaefstathiou, L. L. Yang and J. Zurita, arXiv:1410.3471 [hep-ph]. L. Lehman, arXiv:1410.4193 [hep-ph]. C. Englert, Y. Soreq and M. Spannowsky, arXiv:1410.5440 [hep-ph]. arXiv:1410.6624 [hep-ph].
- [9] S. Willenbrock and C. Zhang, arXiv:1401.0470 [hep-ph].
- [10] Z. Han and W. Skiba, Phys. Rev. D **71** (2005) 075009 [hep-ph/0412166].
- [11] T. Corbett, O. J. P. Ebol, J. Gonzalez-Fraile and M. C. Gonzalez-Garcia, arXiv:1211.4580 [hep-ph]; B. Dumont, S. Fichet and G. von Gersdorff, JHEP **1307**, 065 (2013) [arXiv:1304.3369 [hep-ph]].
- [12] M. Ciuchini, E. Franco, S. Mishima and L. Silvestrini, JHEP **1308** (2013) 106 [arXiv:1306.4644 [hep-ph]].
- [13] A. Pomarol and F. Riva, JHEP **1401** (2014) 151 [arXiv:1308.2803 [hep-ph]].
- [14] J. Ellis, V. Sanz and T. You, JHEP **1407** (2014) 036 [arXiv:1404.3667 [hep-ph]].
- [15] S. Schael *et al.* [ALEPH and DELPHI and L3 and OPAL and SLD and LEP Electroweak Working Group and SLD Electroweak Group and SLD Heavy Flavour Group Collaborations], Phys. Rept. **427** (2006) 257 [hep-ex/0509008].
- [16] V. M. Abazov *et al.* [D0 Collaboration], Phys. Rev. Lett. **109**, 121802 (2012) [arXiv:1207.6631 [hep-ex]].
- [17] S. Chatrchyan *et al.* [CMS Collaboration], JHEP **1306** (2013) 081 [arXiv:1303.4571 [hep-ex]]. ATLAS Collaboration, ATLAS-CONF-2014-010, <http://cds.cern.ch/record/1670531/files/ATLAS-CONF-2014-010.pdf>.
- [18] ATLAS Collaboration, ATLAS-CONF-2013-079, <https://cds.cern.ch/record/1563235/files/ATLAS-CONF-2013-079.pdf>.
- [19] S. Chatrchyan *et al.* [CMS Collaboration], Eur. Phys. J. C **73** (2013) 2610 [arXiv:1306.1126 [hep-ex]]. S. Chatrchyan *et al.* [CMS Collaboration], Phys. Lett. B **721** (2013) 190 [arXiv:1301.4698 [hep-ex]].
- [20] ATLAS Collaboration, ATLAS-CONF-2014-033, <http://cds.cern.ch/record/1728248>.
- [21] A. Falkowski, S. Fichet, K. Mohan, F. Riva and V. Sanz, *Triple gauge couplings revisited*, contribution to the Les Houches 2013 Proceedings, G. Brooijmans, R. Contino, B. Fuks, F. Moortgat, P. Richardson, S. Sekmen, A. Weiler and A. Alloul *et al.*, arXiv:1405.1617 [hep-ph], and to appear.
- [22] M. E. Peskin and T. Takeuchi, Phys. Rev. Lett. **65** (1990) 964 and Phys. Rev. D **46** (1992) 381;

- [23] I. Maksymyk, C. P. Burgess and D. London, Phys. Rev. D **50** (1994) 529 [hep-ph/9306267]. R. Barbieri, A. Pomarol, R. Rattazzi and A. Strumia, Nucl. Phys. B **703** (2004) 127 [hep-ph/0405040].
- [24] G. Altarelli and R. Barbieri, Phys. Lett. B **253** (1991) 161.
- [25] R. Barbieri and A. Strumia, Phys. Lett. B **462** (1999) 144 [hep-ph/9905281].
- [26] R. Contino, M. Ghezzi, C. Grojean, M. Muhlleitner and M. Spira, JHEP **1307** (2013) 035 [arXiv:1303.3876 [hep-ph]].
- [27] J. D. Wells and Z. Zhang, Phys. Rev. D **90** (2014) 033006 [arXiv:1406.6070 [hep-ph]].
- [28] R. S. Gupta, A. Pomarol and F. Riva, arXiv:1405.0181 [hep-ph].
- [29] M. Baak, M. Goebel, J. Haller, A. Hoecker, D. Kennedy, R. Kogler, K. Moenig and M. Schott *et al.*, Eur. Phys. J. C **72** (2012) 2205 [arXiv:1209.2716 [hep-ph]].
- [30] M. Trott, arXiv:1409.7605 [hep-ph].
- [31] C. Grojean, E. E. Jenkins, A. V. Manohar and M. Trott, JHEP **1304** (2013) 016 [arXiv:1301.2588 [hep-ph]]. J. Elias-Mir, J. R. Espinosa, E. Masso and A. Pomarol, JHEP **1308** (2013) 033 [arXiv:1302.5661 [hep-ph]]. J. Elias-Miro, J. R. Espinosa, E. Masso and A. Pomarol, JHEP **1311** (2013) 066 [arXiv:1308.1879 [hep-ph]]. E. E. Jenkins, A. V. Manohar and M. Trott, JHEP **1310** (2013) 087 [arXiv:1308.2627 [hep-ph]]. E. E. Jenkins, A. V. Manohar and M. Trott, JHEP **1401** (2014) 035 [arXiv:1310.4838 [hep-ph]]. R. Alonso, E. E. Jenkins, A. V. Manohar and M. Trott, arXiv:1312.2014 [hep-ph]. J. Elias-Miro, C. Grojean, R. S. Gupta and D. Marzocca, arXiv:1312.2928 [hep-ph]. R. Alonso, H. M. Chang, E. E. Jenkins, A. V. Manohar and B. Shotwell, Phys. Lett. B **734** (2014) 302 [arXiv:1405.0486 [hep-ph]].
- [32] B. Henning, X. Lu and H. Murayama, arXiv:1404.1058 [hep-ph].
- [33] M. Gorbahn, J. M. No and V. Sanz. in preparation.
- [34] A. Alloul, B. Fuks and V. Sanz, arXiv:1310.5150 [hep-ph].
- [35] J. Alwall, M. Herquet, F. Maltoni, O. Mattelaer and T. Stelzer, JHEP **1106**, 128 (2011) [arXiv:1106.0522 [hep-ph]].
- [36] T. Sjostrand, S. Mrenna and P. Z. Skands, JHEP **0605**, 026 (2006) [hep-ph/0603175].
- [37] J. de Favereau *et al.* [DELPHES 3 Collaboration], JHEP **1402**, 057 (2014) [arXiv:1307.6346 [hep-ex]].
- [38] A. Biekötter, A. Knochel, M. Kraemer, D. Liu and F. Riva, arXiv:1406.7320 [hep-ph].
- [39] E. Masso and V. Sanz, Phys. Rev. D **87** (2013) 3, 033001 [arXiv:1211.1320 [hep-ph]].
- [40] A. Djouadi, V. Driesen, W. Hollik and A. Kraft, Eur. Phys. J. C **1** (1998) 163 [hep-ph/9701342].